Searching for Transonic Aeroelastic Instability Using an Aerodynamic Model Hierarchy

S. Timme* and K. J. Badcock†

University of Liverpool, Liverpool, England L63 3GH, United Kingdom

A hierarchy of flow models is exploited for transonic aeroelastic stability analysis using the kriging interpolation technique applied within the Schur complement eigenvalue framework. In the Schur framework a modified structural eigenvalue problem describes the coupled aeroelastic system with a pre–computed interaction term depending on the response frequency. The interaction term, representing the influence of the high–dimensional computational fluid dynamics system, is approximated by reconstruction based on samples which can be computed using a frequency or time domain solver. The computationally cheap approximation model is developed and discussed in this paper for two degree–of–freedom aerofoil cases. Also, the approximation model is used both for blind search of aeroelastic instability and for updating predictions based on aerodynamic models of different fidelity.

I. Introduction

Two capabilities missing from the aerodynamic modelling tools available for aeroelasticity are a general method to update lower order models with better information as this becomes available, and an approach to assessing the impact of uncertainties in the prediction of aerodynamic phenomena like shock waves and regions of separation. Simple parameterised models are used in structural dynamics to facilitate both of these types of analysis [1] and experiments are exploited to tune the parameters to match observations. The sensitivity to parameters can be easily assessed. In aerodynamics using linear tools in the frequency domain (e.g. Doublet Lattice Method), various approaches have been discussed in the literature focusing on correcting the aerodynamic influence coefficient matrix with nonlinear data [2]. When nonlinear flow models are concerned, there are neither well established methods for exploiting measured data or higher order predictions, nor systematic ways to assess the impact of uncertainties on the aeroelastic behaviour. The current paper describes an investigation into developing a method that will address these shortcomings for the limited case of transonic aeroelastic predictions for an aerofoil configuration moving in pitch and plunge.

The understanding of physical mechanisms in aeroelastic simulations would be assisted by the ability to consider the impact of uncertainty and sensitivity. In structural dynamics methods to assess the impact of uncertainty in model parameters are well established [1, 3]. For instance a probability distribution in one (or many) input parameters is propagated through the simulation and the effect on the system dynamics is investigated. Propagation tools such as interval analysis, perturbation and polynomial chaos methods, or even brute force Monte Carlo simulations, are routinely used. In recent years these tools have started to be transferred to computational fluid dynamics (CFD). As an early example, the authors of [3] investigated several propagation methods to address parametric uncertainty for the nonlinear Burgers' equation. Approaches considering uncertainties in the physical modelling assumptions rather than the parameters are rare though. Examples of dealing with uncertainties in the boundary treatment of a physical model include, for instance, a geometrically uncertain domain boundary for the two–dimensional Laplace equation [4], and both deterministic and random perturbations on the boundary condition for the viscous Burgers' equation subject to sensitivity to the boundary data [5].

*Research Engineer, CFD Laboratory, Department of Engineering, sebastian.timme@liverpool.ac.uk.

†Professor, CFD Laboratory, Department of Engineering, K.J.Badcock@liverpool.ac.uk, Senior Member AIAA.

As pointed out in [6], uncertainty associated with the aerodynamic model can be considerably larger than from the structural model. Also, transonic aerodynamics introduce nonlinearity into the aeroelastic dynamics. Two aeroelastic phenomena are particularly associated with the nonlinear flowfield. One is the transonic dip where the presence of shock waves reduces the stability of the aeroelastic system. The second is limit–cycle oscillation (LCO) where the limiting mechanisms of the amplitude of the dynamic response are shock motions and separation. In [7] the influence of aerodynamic modelling assumptions on the amplitude of a store–induced LCO was investigated for the Goland wing. The dependence of LCO amplitudes on the modelling level, considering both inviscid and viscous flow, was investigated. It was argued that shock/boundary layer interaction in this case causes trailing edge separation and retards the shock movement (substantial in the inviscid case otherwise) thus limiting the LCO amplitude. Modelling both the inviscid/viscous interaction as well as the extent of the shock–induced separated regions is therefore important.

An important contribution to the understanding of transonic LCO is the experimental studies of the supercritical NLR 7301 aerofoil [8–10]. The impact of shock/boundary layer interaction on LCO amplitude and the importance of the correct prediction of the steady state solution are discussed and conclusions drawn for the required aerodynamic modelling fidelity. A comprehensive review of nonlinear aeroelastic phenomena including a detailed discussion of possible physical sources for these nonlinearities is given in [11].

The stability of an aeroelastic system can be inferred from time–accurate simulations following an initial excitation of the system. Calculations of complete aircraft configurations have been made [12, 13]. The time–accurate approach is very capable due to its generality. However, the significant computational cost, in particular to solve for the unsteady, nonlinear transonic aerodynamics, is a major drawback of this approach. A requirement to search a space of system parameters and flight conditions for critical conditions makes this situation worse. The issue of cost generally limits the analysis to a few carefully chosen cases. Alternative approaches have been investigated to obviate the computational costs and to permit routine calculations over larger parameter ranges [14]. One popular method is reduced order modelling (ROM) based on proper orthogonal decomposition (POD). For a robust and reliable ROM to exist, the parameter space and flow phenomena of interest have to be covered by the set of system responses used to establish the ROM, and thus, creating the large number of system responses is the main cost. In addition, the reliability of the POD/ROM approach under parameter changes is a topic of investigation [15]. A variant of the POD technique was applied both to deal with incomplete data in the reconstruction of aerodynamic flow fields and to provide a link in updating numerical predictions with experimental measurements [16].

An alternative approach discussed in the present work uses the theory of dynamical systems to predict aeroelastic instability of the Hopf type commonly leading to flutter and LCO. Here, a stability problem for a steady state solution of the aeroelastic system is examined instead of performing unsteady simulations. Stability is lost by a Hopf bifurcation when a pair of complex conjugate eigenvalues of the system Jacobian matrix crosses the imaginary axis for some value of a critical system parameter. Following an approach first published in [17–19], the bifurcation method was successfully tested on a two–dimensional aerofoil configuration free to move in pitch and plunge. Convergence problems associated with applying a direct solver to a large linear system were resolved by using an iterative sparse linear solver [20]. The method was extended to a larger problem investigating a flexible AGARD 445.6 wing using a modal structural model [21]. Later, the shifted inverse power method was adapted to allow tracing of the critical eigenvalues with changing values of the system parameter. This provides information about the damping and frequency of the aeroelastic modes [22]. Also, a model reduction technique based on the centre manifold theory was investigated to simulate an LCO response in the vicinity of the linear instability point [22].

An improved version of the basic method used a Schur complement eigenvalue formulation to enhance computational performance [23] and was applied to several wing structures and also complete aircraft configurations to study uncertainty in the predicted instability due to structural variability [24]. This approach views the coupled aeroelastic system as a modified structural eigenvalue problem with the interaction (correction) term, which depends on the response frequency, pre–computed. In the current paper the approximation of this interaction term is formulated so that a hierarchy of aerodynamic models can be exploited, with cheaper models being used to evaluate possible conditions of interest for more expensive models, whose evaluations are then used to update the approximation.

The paper continues with the formulation and benchmarking of the aerodynamic and aeroelastic tools. The generation of the interaction term and its approximation using the kriging interpolation technique are then considered, and an aeroelastic stability analysis for a pitch and plunge aerofoil is presented to illustrate

the approach. Finally, ideas for coordinated sampling and model updating to assist the construction of the approximation model applied to the stability analysis are investigated.

II. Models

In [25] four main aerodynamic modelling levels are discussed; linear and nonlinear potential, Euler and Navier–Stokes. The physics in the simulation can be built up from linear potential flow. The nonlinear potential model adds nonlinear compressible flow effects. Then, the Euler equations add entropy and vorticity effects, while the Navier–Stokes equations include viscous and heat–conducting effects. For aerodynamic flows of practical interest, the Reynolds–averaged form of these equations (RANS) is generally used introducing the requirement for turbulence models. In the current paper, the RANS equations, the Euler equations as well as the unsteady nonlinear full potential equations with and without coupling of an integral boundary layer formulation are considered as aerodynamic models, while an eigenvalue–based module, details of which are given in the next section, is used to evaluate aeroelastic stability.

The RANS and Euler equations are solved using an established research code [26]. Basic features of the code include; spatial discretisation done by a block–structured, cell–centred, finite–volume scheme, implicit time marching applied for steady state solves, second order dual time stepping used for unsteady simulations [27], convective fluxes evaluated by the approximate Riemann solver of Osher and Chakravarthy [28] with the MUSCL scheme [29] achieving essentially second order accuracy and van Albada's limiter preventing spurious oscillations around steep gradients, and viscous fluxes evaluated by central differences. The resulting linear systems are solved by a preconditioned Krylov subspace iterative method. Boundary conditions are enforced using two layers of halo cells. Linear eddy viscosity turbulence models used in this work are solved in a fashion similar to the RANS equations with source terms being evaluated at cell centres.

The continuity and Bernoulli equations constitute the unsteady full potential model (FP) solved by a newly developed research code [30]. Basic features of the code include; spatial discretisation done by an unstructured triangular, vertex–based, finite–volume scheme, Newton's iterative method applied for steady state solves, second order dual time stepping used for unsteady simulations [27], and convective fluxes evaluated by a second order, slope–limited, gradient–based upwind scheme using a linear least squares reconstruction. Linear systems are solved by a direct solver [31]. The potential jump (i.e. circulation), based on the Kutta condition, is applied across the wake cut and is convected downstream in the usual unsteady fashion [32]. Boundary conditions are set using a layer of halo vertices with a transpiration boundary condition applied at solid walls. Viscous effects (FPv) are added to the basic model using an integral boundary layer formulation [33–36] derived from the unsteady Prandtl boundary layer equations [37]. Additional unknowns of the integral system are expressed in terms of the primary unknowns using closure correlations. The "blowing velocity" concept is applied to model the leading order effect of the viscous layer, displacing the outer inviscid flow by a distance equal to the displacement thickness [38].

Results for one standard test case are presented to build confidence in the developed FPv flow solver. Steady measurements of pressure distributions in sub- and transonic flow regimes are given in the experimental data base of [39] for the supercritical RAE 2822 aerofoil. Results are shown in Fig. 1 for cases 2 (subsonic) and 9 (transonic). The simulations were done assuming free flight conditions. Hence, the numerical flow conditions were adjusted to match the experimental data subject to wall interference effects. The FPv simulations give excellent agreement to the experiments and the RANS results.

The structural part in the aeroelastic problem is described by the dynamics of a two degree–of–freedom aerofoil [40]. The "typical section" aerofoil with oscillating pitching and plunging motion represents the torsional and bending behaviour of a wing structure. The linear model is idealized as a point mass located at the centre of gravity as well as a torsional and a translational spring attached to the elastic centre located some distance away from the centre of gravity.

III. Generating the Schur Interaction Matrix

A. Schur Complement Eigenvalue Formulation

Write the aeroelastic system in semidiscrete notation as $\dot{\boldsymbol{w}} = \boldsymbol{R}(\boldsymbol{w}, \mu)$, where the vector of unknowns $\boldsymbol{w} = [\boldsymbol{w}_f, \boldsymbol{w}_s]^T$ contains fluid and structural contributions, and $\boldsymbol{R}$ is the corresponding residual vector. The system depends on an independent parameter μ representing, for instance, dynamic pressure or altitude. An

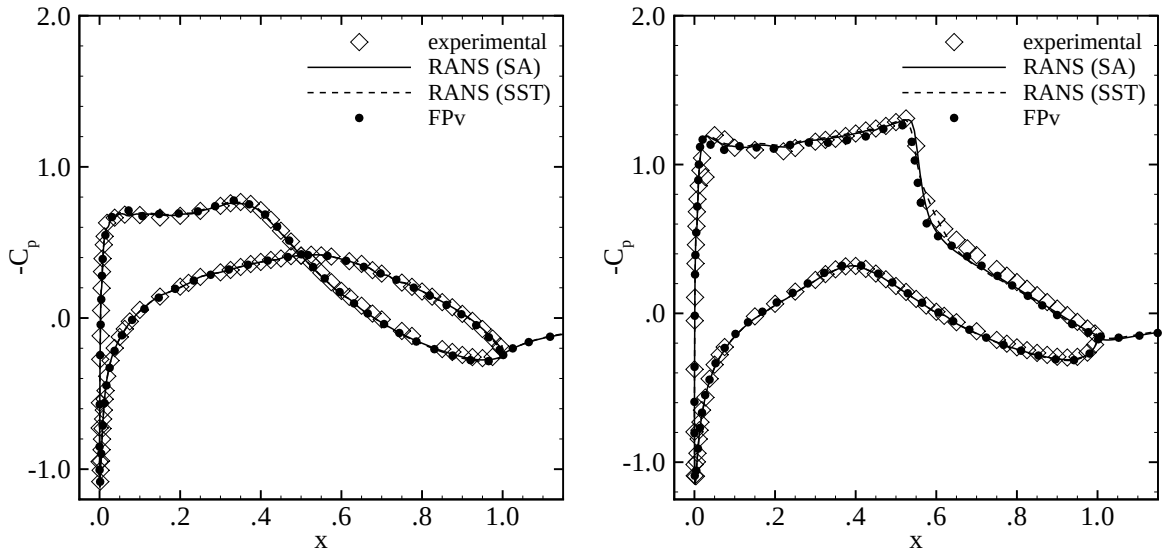

(a) Case 2 (M=0.685, α=$-2.35°$, Re=5.7×10^6) (b) Case 9 (M=0.735, α=$2.80°$, Re=6.5×10^6)

Figure 1. Pressure distributions of RAE 2822 aerofoil showing comparisons of measurements as presented in [39] and simulations using RANS and FPv.

equilibrium solution $\bar{\boldsymbol{w}}$ of the nonlinear system satisfies $\boldsymbol{R}(\bar{\boldsymbol{w}}, \mu) = 0$. The theory of dynamic systems gives criteria for an equilibrium to be stable. In particular, stability is determined by eigenvalues, $\lambda = \sigma \pm i\omega$, of the system Jacobian matrix $A(\bar{\boldsymbol{w}}, \mu)$ evaluated at the steady state and arbitrary values of μ. A stable system has all its eigenvalues with a negative real part. In many aeroelastic problems a pair of complex conjugate eigenvalues with zero real part defines the onset of an instability of the Hopf type leading to flutter and LCO. Linear stability is predicted by solving the general eigenvalue problem, $(A - \lambda I)\,\boldsymbol{p} = 0$, where the Jacobian matrix is conveniently partitioned in blocks expressing the different dependencies

$$A = \frac{\partial \boldsymbol{R}}{\partial \boldsymbol{w}} = \begin{pmatrix} A_{ff} & A_{fs} \\ A_{sf} & A_{ss} \end{pmatrix}. \tag{1}$$

For convenience, also the eigenvector $\boldsymbol{p}$ is partitioned into unknowns corresponding to fluid and structural contributions [23]. Then, the Schur complement eigenvalue formulation is given as $S(\lambda)\,\boldsymbol{p}_s = 0$, which is a small nonlinear eigenvalue problem. The Schur complement matrix $S(\lambda)$ is explicitly written as

$$S(\lambda) = (A_{ss} - \lambda I) - A_{sf}\,(A_{ff} - \lambda I)^{-1} A_{fs}. \tag{2}$$

The first term on the right–hand side defines the structural eigenvalue problem and is denoted as $S^s = A_{ss} - \lambda I$, while the second part constitutes the interaction (coupling) term $S^c = -A_{sf}\,(A_{ff} - \lambda I)^{-1} A_{fs}$. To solve this small complex–valued eigenvalue problem, the system is augmented to scale the structural eigenvector $\boldsymbol{p}_s$ against a real–valued constant vector $\boldsymbol{c}_s$, i.e. augment by the equation $\boldsymbol{c}_s^T \boldsymbol{p}_s - i = 0$. Then, the augmented nonlinear system is solved for the unknowns $[\boldsymbol{p}_s, \lambda]^T$. While the full eigenvalue formulation solves a problem with $n_f + 2n + 1$ unknowns, the Schur formulation only has $2n + 1$ where the number n of relevant normal modes is generally small. There are several ways to evaluate the roots of the Schur residual as outlined in the following and with more details given in [23, 24].

An efficient way of finding the roots of nonlinear systems are Newton–like methods which require forming the residual and its Jacobian matrix. The main cost in either method is to evaluate the interaction term S^c since it includes operations on the high–dimensional fluid system, whereas the costs to form the structural term S^s are negligible. Using *Newton's method*, the interaction term in the Schur residual is conveniently evaluated by first forming the product $A_{fs}\,\boldsymbol{p}_s$ for the current approximation to the eigenvector, and then solving one linear system, $(A_{ff} - \lambda I)\,\boldsymbol{y} = A_{fs}\,\boldsymbol{p}_s$. The solution is multiplied against matrix A_{sf}. Applying finite differences gives the Jacobian matrix where multiple evaluations of the residual are required.

There are n relevant solutions of the nonlinear eigenvalue problem, and so the cost of forming the interaction term at each Newton iteration for each value of the independent parameter becomes too high. To overcome this, a series approximation [41] of the Schur complement matrix can be written for $\lambda = \lambda_0 + \lambda_\varepsilon$ as

$$S(\lambda) \approx (A_{ss} - \lambda I) - A_{sf} \left(\left(A_{ff} - \lambda_0 I\right)^{-1} + \lambda_\varepsilon \left(A_{ff} - \lambda_0 I\right)^{-1} \left(A_{ff} - \lambda_0 I\right)^{-1} \right) A_{fs}, \tag{3}$$

where λ_ε is a small variation to the reference value λ_0, which is a normal mode frequency or a previous converged solution. Pre–computing the factors in the series against the matrix A_{fs} (requiring $4n$ linear solves per normal mode frequency λ_0), allows the application of the expansion in the vicinity of λ_0. Two approaches have been discussed. The *quasi–Newton method* evaluates the (exact) residual by the nonlinear approach given in the previous paragraph, while the series is used for the Jacobian matrix. The *series method* also applies the series expansion to the residual which is possible for small λ_ε and for an independent parameter μ not affecting the pre–computed values.

In this work, as discussed in the next section, a new method is introduced. The Schur residual and the Jacobian matrix are formed by approximating the Schur interaction term S^c by a reconstruction based on samples, i.e. full order evaluations of this term, covering the parameter space of interest.

For the structural model of the two degree–of–freedom aerofoil, a 4×4 Schur complement matrix is found. There are six nonzero complex–valued elements in the interaction term. Ordering the structural unknowns of plunge h and pitch α as $\boldsymbol{w}_s = [h, \dot{h}, \alpha, \dot{\alpha}]^T$, the first and third row (due to the matrix A_{sf} projecting the fluid response onto the structural states) as well as the first column (due to the independence of the fluid response on the plunge state h) are zero within the matrix.

B. Extracting Elements based on Fourier Series

The interaction matrix can be formed in both the frequency and time domain. Solving the $2n$ linear systems (one for each column of the matrix A_{fs}) against the fluid system directly to form the Schur interaction matrix is referred to as the linear frequency domain approach. Alternatively, the interaction matrix is evaluated from a Fourier analysis of unsteady responses forced in the structural states. Therefore, the unknowns are rearranged as the sum of a steady state solution $\bar{\boldsymbol{w}}$ and a corresponding unsteady perturbation $\delta \boldsymbol{w}$. Writing the fluid part of the aeroelastic system in its time–linearized form,

$$\dot{\boldsymbol{w}}_f = A_{ff}\, \delta \boldsymbol{w}_f + A_{fs}\, \delta \boldsymbol{w}_s, \tag{4}$$

with the Jacobian matrix blocks A_{ff} and A_{fs} evaluated at the steady state, and expressing the unsteady perturbation of the fluid and structure in a truncated exponential Fourier series [42], a discrete expression can be given as,

$$\sum_{n=-N}^{N} \boldsymbol{\alpha}_n = - \sum_{n=-N}^{N} \left(A_{ff} - i\, n\, \omega I\right)^{-1} A_{fs}\, \boldsymbol{\beta}_n. \tag{5}$$

The complex–valued Fourier coefficients ($\boldsymbol{\alpha}_n$ for fluid response and $\boldsymbol{\beta}_n$ for structural forcing) are evaluated from the time signal over a period $T = 2\pi/\omega$ (with ω as the fundamental frequency). After multiplying with the Jacobian matrix block A_{sf} (evaluated analytically or by finite differences), the expression in Eq. (5) corresponds to the interaction term for an undamped eigenvalue with column and magnitude set by the applied structural forcing. Evaluating the Fourier coefficients at integer multiples n of the fundamental frequency (provided the system was excited accordingly) gives the interaction matrix at these discrete frequencies. Solutions of a fully nonlinear system approach the time–linearized results if the amplitude of the forced motion is sufficiently small, i.e. the unsteadiness in the flow is linearly dependent on the structural motion. The step of using the nonlinear system is required if the Jacobian matrices for the fluid contribution are not available explicitly (otherwise the linear frequency domain approach should be used).

An example to illustrate the different generation methods is presented next. A NACA 0012 aerofoil configuration defined in [20] as the "heavy case" was excited in all structural states of interest simultaneously in sinusoidal motions at a fundamental frequency of $\omega = 0.15$ and an amplitude of $\hat{a} = 1.0 \times 10^{-4}$. Three simulations were required to obtain the interaction matrices at three frequencies while swapping around the factors multiplying the fundamental frequency to have distinct excitations in the structural states. Exciting the plunge coordinate h is irrelevant. Following the transition to stable periodic cycles, one motion cycle simulated with 128 steps is used for evaluating the Fourier coefficients. Two freestream Mach numbers are considered representing a sub- and a transonic case with a strong shock wave. Figure 2, showing real

and imaginary parts individually, gives an excellent agreement in evaluating an element of the interaction matrix. Summarizing the costs, the linearized time domain approach involves the costs of about 10 steady state simulations to extract the complete interaction matrix at one individual frequency, while the nonlinear version is about twice this cost. Using the linear frequency domain approach, on the other hand, evaluating the interaction matrix at one frequency (requiring $2n$ linear solves against the fluid system) takes about an equivalent cost to simulating a steady state.

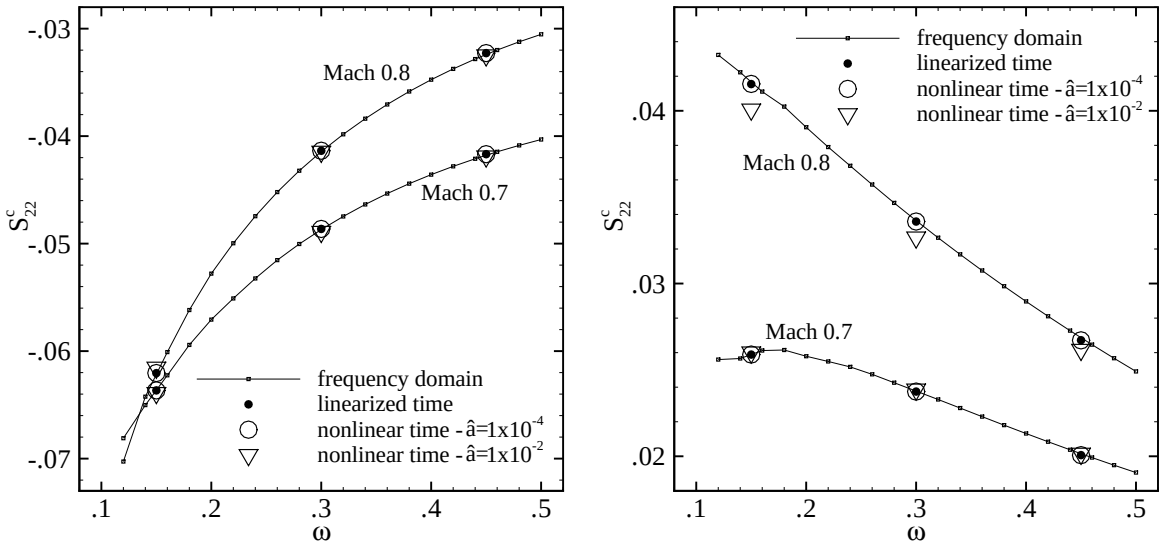

(a) Element real(S^c_{22}) of interaction matrix

(b) Element imag(S^c_{22}) of interaction matrix

Figure 2. Extracted element of Schur interaction matrix for Euler flow model and NACA 0012 configuration showing real and imaginary parts individually; linearized and nonlinear time–domain compared to linear frequency domain.

Figure 2 also includes nonlinear time domain results of a higher excitation amplitude ($\hat{a} = 1.0 \times 10^{-2}$). Intuitively, the results at Mach 0.8 suggest that the nonlinear approach loses accuracy compared to the linear approaches. However, the appearance of shock waves introduces the additional aspect of an oscillatory behaviour as discussed in [43]. Therein, the critical flutter speed index of an aerofoil configuration showed an oscillatory trend with changes in freestream Mach number due to the discrete numerical representation of the shock movement being restricted to the grid resolution. The oscillatory flutter speed was related to an oscillation in the Jacobian matrix elements. Figure 3 presents such nonlinear time domain results using Euler and RANS flow models at a range of Mach numbers and different amplitudes $\hat{a}$. In Fig. 3(a) the Euler time domain results are compared to linear frequency domain predictions. As discussed in [43] for the influence of an initial disturbance on unsteady simulations, a dependence on the amplitude can be found. Results for small excitation amplitudes resemble the linear frequency analysis including the oscillatory phenomenon, whereas higher values eliminate these. A weak variation of the pressure distribution is found for small structural motion amplitudes with a strong influence of the discrete steady state shock resolution throughout the unsteady forcing. The dynamic effects due to larger amplitudes, on the other hand, dominate the influence of the steady state. Physically, it seems to be more meaningful to use a higher excitation amplitude since the nonsmooth behaviour, which cannot be explained with arguments of a continuous change of a system parameter, disappears.

Comparing steady state lift coefficients for Euler and RANS flow models suggests that the phenomenon can also be expected for RANS simulations. Figure 3(b) distinguishes three regions. In shock free flow at sub- and very low transonic Mach numbers, the amplitude (chosen within reason) is irrelevant. Having a distinct shock wave, the forcing amplitude becomes an important factor as for the Euler simulations. Results for smaller amplitudes scatter around a mean value, while the results for higher amplitudes, leaving the constraints of the discrete grid resolution, show a converging trend in the evaluations. A trend for the region of distinct shock–induced flow separation starting at about Mach 0.82 is less easy to establish. While the presented matrix element describes significant oscillations, other elements have a far more gentle

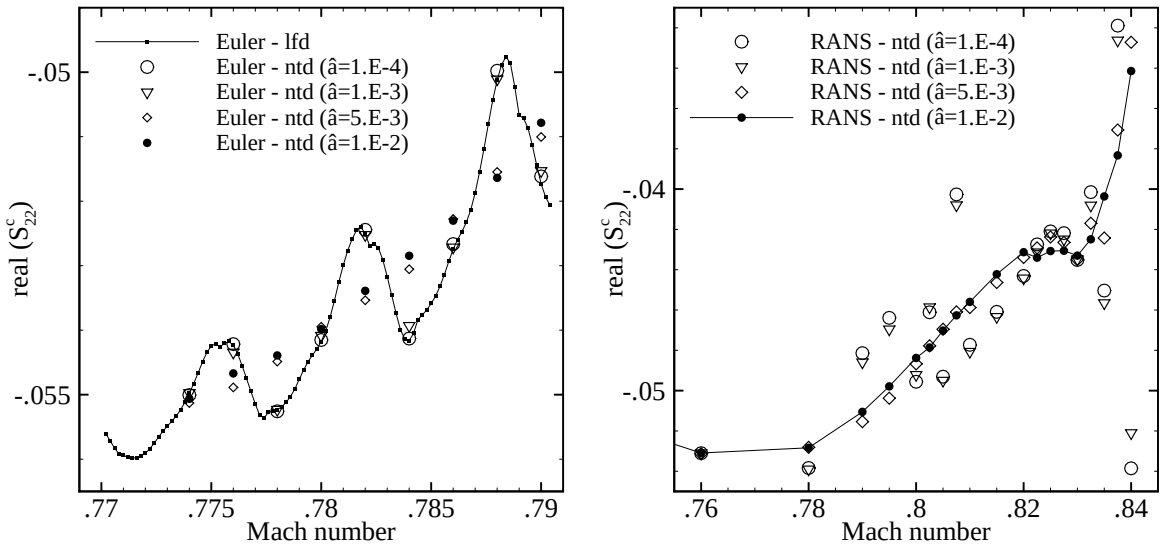

(a) Euler flow model

(b) RANS (SST) flow model

Figure 3. Effect of excitation amplitude on oscillatory behaviour in transonic regime for element real(S^c_{22}) of the interaction matrix showing results for different flow models and a frequency of $\omega = 0.25$.

development. Additionally, the forced excitation with higher amplitude may cause severe flow separation challenging a linear relationship between the fluid response and structural motion. To understand these points, the stability at Mach 0.84 has been analysed by means of the kriging–based approach, described in the following, as well as time–accurate simulations following a disturbance of the steady state. While time–accurate results agree in the stability prediction with the analysis based on the higher amplitude samples, the lower amplitude samples give a relative error of about 10 percent.

IV. Approximating the Schur Interaction Matrix

A. Overview of Kriging Interpolation Techniques

For computationally expensive simulations it is useful to generate a cheap approximation based on relatively few runs of the expensive model to provide information about its response at untried parameter combinations. An approximation model should both predict the calculated responses precisely and adapt to the functional behaviour of the responses. In the kriging (nonlinear least squares) interpolation technique a multidimensional deterministic response of a simulation is treated as a realisation of a stochastic process composed of a low order regression model and a random normally distributed signal with zero mean and a covariance depending on the variance of the input samples and the correlation between two parameter locations. Thus, the second term (the error term) is not independent at different locations but is related to the distance between points in the parameter space. The parameters of the computationally cheap kriging model are determined for a known set of numerical samples of the full order formulation by an optimisation process as given, for instance, in [44, 45]. The kriging predictor gives the exact system response at a sample location. Previously, the kriging approximation was used for generating aerodynamic data applied in flight dynamics studies [46].

Co–kriging techniques use additional information on the functional behaviour of the response, such as gradients or co–variables. Using a spatially correlated, (usually) cheaper, and hence densely sampled co–variable to augment the input parameter space of a (usually) more expensive, sparsely sampled primary variable, allows the prediction of the primary variable accurately with very few samples. The cheaper model provides a trend of the system response with the higher fidelity data updating the prediction [45]. In this context the cheaper model is established either by a lower level aerodynamic modelling (which exploits the aerodynamic hierarchy of flow models) or by a higher level model solved on a coarse grid.

B. The Kriging Predictor applied to Aeroelastic Stability Analysis

Evaluating the Schur interaction matrix S^c based on the full order formulation accounts for the highest cost in the stability analysis. Once the approximation model based on full order samples is evaluated, the stability problem is solved without relying on the exact solver, and thus, becomes very cheap. Then, any Newton–like method is a convenient choice to solve the nonlinear stability problem with the interaction term and its Jacobian matrix readily available through the kriging predictor. The critical eigenvalue with zero damping is detected using the bisection method applied to the independent (bifurcation) parameter at fixed Mach number.

In the current formulation the approximation of the interaction term is based on a purely imaginary eigenvalue with zero damping $\lambda = i\,\omega$, whereas the structural part uses the complete eigenvalue including nonzero real part.[a] In this sense it is an analogy to the classical $p-k$ method [47]. The approximate Schur complement matrix used for the stability analysis is written as

$$S = S^s(\lambda, \bar{u}) + \hat{S}^c(\omega, M) \tag{6}$$

where $\hat{S}^c$ is the kriging prediction of S^c and M denotes the Mach number. Interestingly, for the two degree–of–freedom aerofoil discussed in the present study the correction term S^c is independent of the bifurcation parameter, given by the reduced velocity $\bar{u}$, thus simplifying the discussion. At the critical eigenvalue $\lambda_F = i\,\omega_F$ the approximation is exact within the limits of the interpolation algorithm.

Figure 4 shows the tracing of the least stable aeroelastic mode for the "heavy case" NACA 0012 configuration using the Euler flow model. The calculation of 60 points on the root locus took less than a second of CPU time with the approximation model, whereas the full formulation having a grid with 15k control volumes took more than an hour (about one minute per point) on a modern desktop personal computer using the *quasi–Newton method*. Unsteady time marching at an individual reduced velocity using a dimensionless time step of 0.05 for temporal accuracy takes about 13 minutes per motion cycle (comprising about 500 steps). Two approximation models are shown with the samples extracted using the linear frequency domain approach. One, denoted as "approx (w/o damping)", used full order samples with zero damping and varying frequency, whereas the second one was constructed at fixed Mach numbers for both varying damping and frequency. Using the approximation model based on nonzero damping, the trace of the relevant eigenvalue follows the full order prediction precisely. However, the eigenvalue can be traced quite accurately even away from the imaginary axis without including damping in the kriging predictor. In this case the error introduced by the approximation $\hat{S}^c(\omega, M)$ is very small in the relevant region close to the imaginary axis suggesting that the variation of the interaction elements with damping (or at least that the influence of this variation on the eigenvalue problem) is small compared to the structural part $S^s(\lambda, \bar{u})$.

Figure 5 presents the sub- and transonic instability boundary as critical values of flutter speed index $V_F = \bar{u}_F/\sqrt{\mu_s}$ (where μ_s is the aerofoil–to–fluid mass ratio) and frequency ω_F for the NACA 0012 configuration. A comparison of results from the full order and the approximation models is given for four aerodynamic modelling levels. Also, since the eigenvalue–based full order formulation is not available, time–accurate simulations to confirm the RANS predictions (using a chord Reynolds number of 5 million) are included with the plus (tilde) sign indicating a stable (unstable) response due to an initial disturbance. The agreement is excellent as should be expected since the sample resolution is high. The samples for a range of Mach numbers and frequencies (with zero damping) and the corresponding kriging evaluations are shown in Fig. 6 for one element of the interaction matrix. The trace of the instability is included as combinations of Mach number and critical frequency to illustrate the important regions of the response surface. The samples were extracted using either the linear frequency domain or, for the RANS simulations, the nonlinear time domain approach with an excitation amplitude of 7.75×10^{-3} applied.

C. Interpreting the Results for Different Flow Models

In Fig. 5 there is a constant offset between Euler and RANS results as well as (at least for lower Mach numbers) between FP and FPv results suggesting that the boundary layer as predicted by viscous modelling levels has a stabilizing effect on the configuration. Furthermore, it seems that the shock dynamics, which

[a] One contribution is missing in the reduced formulation compared to the full version. The structural part S^s contains terms involving $\partial C_l/\partial\alpha$, $\partial C_m/\partial\alpha$, etc., i.e. the dependence of the structural residual on the structural unknowns through aerodynamic forces. These missing contributions are very small as shown by the comparisons below. The uncertainty due to the interpolation algorithm is considered to be far more significant.

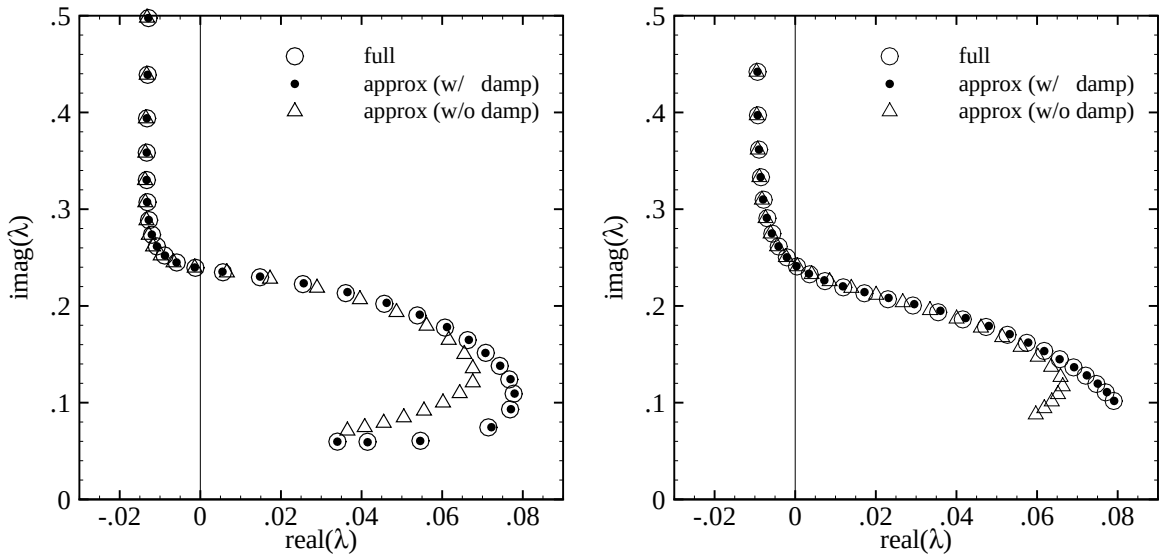

(a) Mode tracing at Mach 0.7

(b) Mode tracing at Mach 0.8

Figure 4. Mode tracing of least stable mode for NACA 0012 configuration using Euler flow model; comparison of full order and approximation models with damping terms $\hat{S}^c(\lambda)$ and without damping terms $\hat{S}^c(\omega)$.

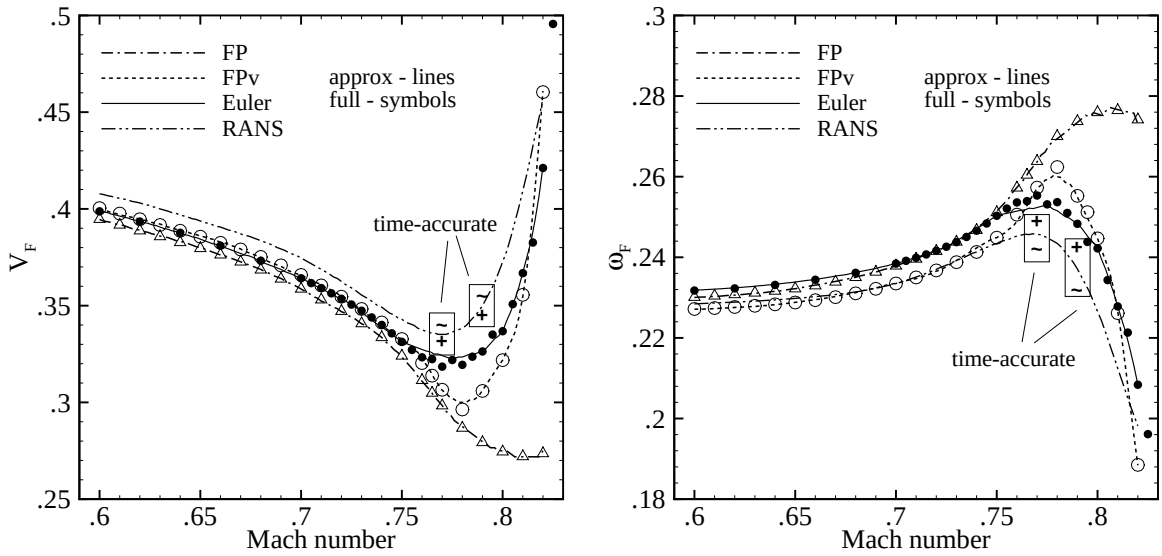

(a) Critical flutter speed index

(b) Critical frequency

Figure 5. Instability boundary for NACA 0012 configuration for four levels of aerodynamic modelling showing comparison of full order (full) and approximation models (approx).

are correctly predicted by the Euler model, act as the dominant mechanism for the aeroelastic instability compared to the viscous effects (in this configuration and at the shown range of Mach numbers). Indeed, comparing flow solutions it can be seen that shallow separation due to shock/boundary layer interaction is first encountered at about Mach 0.81 to 0.82.

The response surfaces of the interaction matrix element shown in Fig. 6 for the different flow models are now interpreted. To start with, it is found that the flow models produce similar response features which should be expected since the shock dominated physics are included in all flow descriptions while separation is not yet an important factor in the considered Mach number range. In the subsonic range the flow response (as

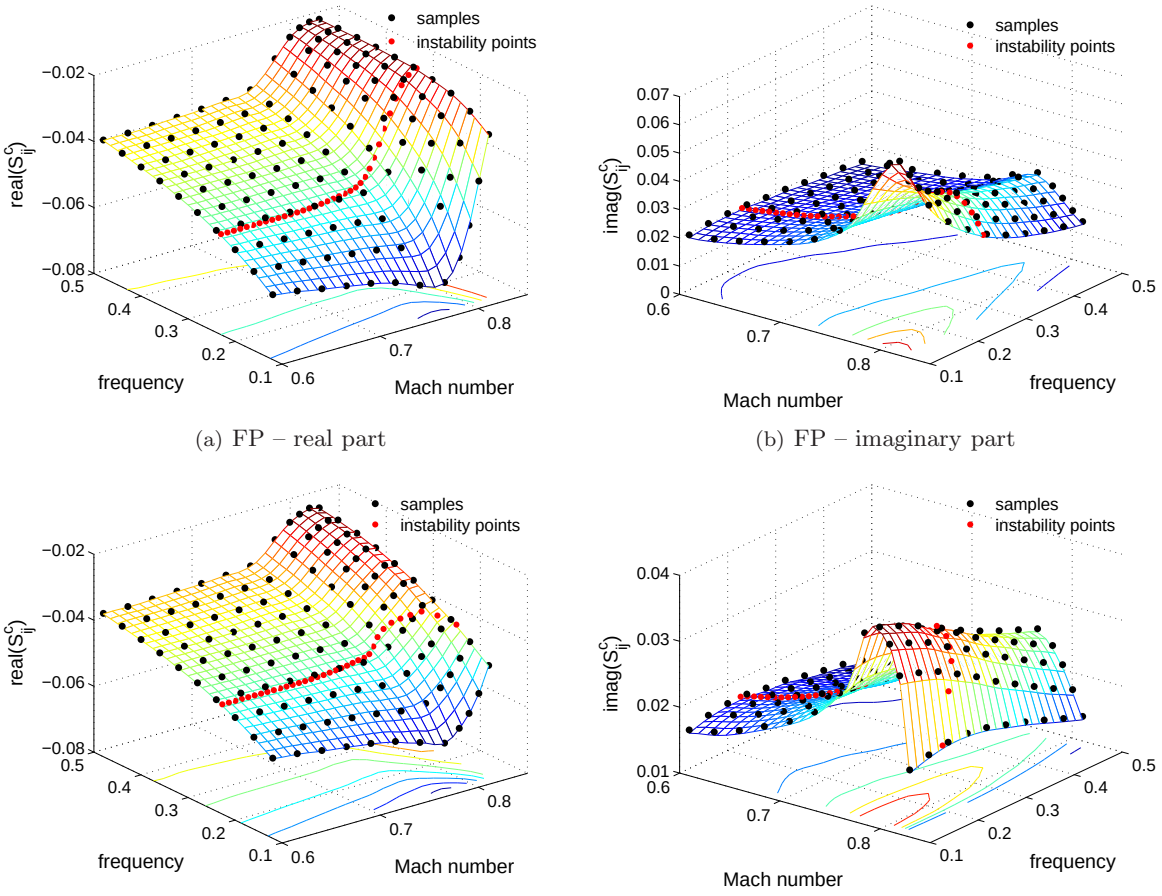

(a) FP – real part

(b) FP – imaginary part

(c) FPv – real part

(d) FPv – imaginary part

Figure 6. Extracted and interpolated element S^c_{22} of Schur correction matrix for NACA 0012 configuration including real and imaginary parts and using four levels of aerodynamic modelling.

expressed by the matrix elements) has small changes with varying system parameters, while in the transonic range clear variations, in particular with respect to the Mach number, are present. One distinct difference is found for the FP flow model at the higher Mach numbers and smaller frequencies. Here, the imaginary part of the shown element takes on values almost double the elements of the other models which is likely due to the shock dynamics (including location and strengths) being incorrectly predicted. This suggests that, once the correct response features are simulated reasonably well by models with different fidelity, a hierarchy of flow models can be exploited in the stability analysis by combining cheaper response evaluations with available better (more expensive) information.

Differences in the stability prediction using the different flow models require further consideration. Even for subsonic Mach numbers an offset between both the inviscid (Euler vs FP) and the viscous (RANS vs FPv) predictions of the critical flutter speed index can be found (even though the approximated error of one percent should not be of too much concern). The reason for disagreement is not found to be the grid resolution since the results presented herein are grid–converged meaning that inspected finer grids (results of which are not shown) did not change the results notably. An important factor distinguishing the solver for Euler/RANS and FP/FPv flow models are the distinct spatial discretisation schemes including the treatment of boundary conditions. For instance, the FP baseline solver using a time–invariant computational domain applies a transpiration boundary condition on solid surfaces, whereas in the multiblock solver for the Euler/RANS equations the geometry is explicitly deflected. These distinct boundary treatments are considered next.

Since a FP formulation with moving grids is currently not available, a transpiration boundary condition was implemented in the Euler formulation. The transpiration boundary condition only affects the Jacobian matrix block A_{fs} in Eq. (1) and implementing this (using finite differences) is easily done. The results shown

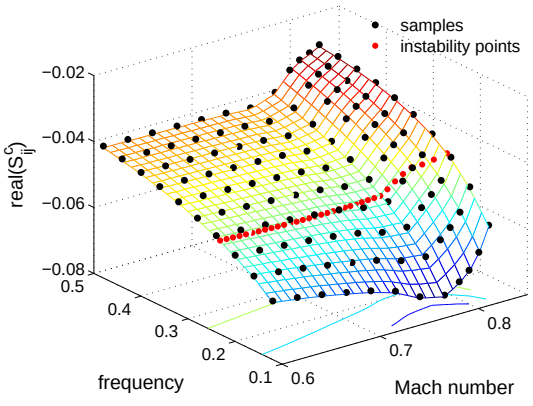

(e) Euler – real part

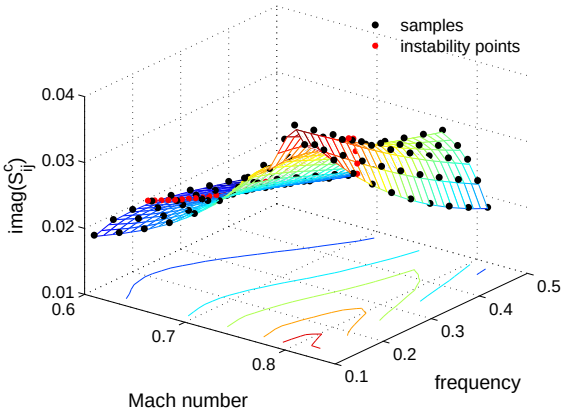

(f) Euler – imaginary part

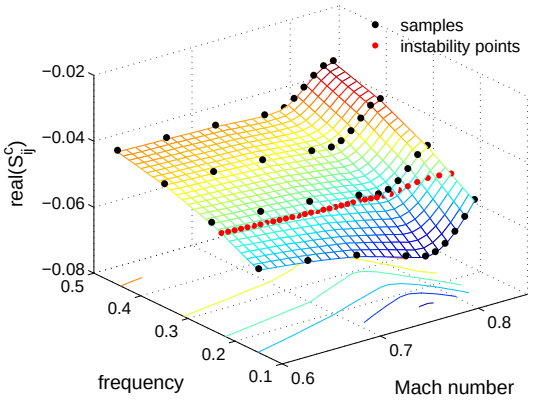

(g) RANS – real part

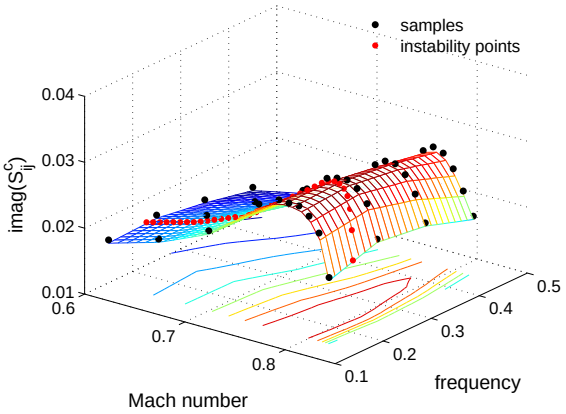

(h) RANS – imaginary part

Figure 6. (con't)

in Fig. 7(a) indicate that the modified boundary condition has a slight influence on the aeroelastic stability. Compared to the original results the critical flutter speed index approaches the FP prediction.

The critical flutter speed index of the FP formulation is closely followed until about Mach 0.75. Intuitively, starting from this point one would point at the underlying FP modelling assumptions being violated by the formation of strong shock waves causing an underprediction of the transonic dip. (The critical Mach number of the NACA 0012 aerofoil is at about 0.73.) However, the steady pressure distributions at Mach 0.78 shown in Fig. 8 give excellent agreement for both the viscous and the inviscid flow solutions. These results suggest that merely an accurate simulation of the steady flow field is not sufficient with additional physical sensitivities such as entropy and vorticity effects due to shock waves becoming more and more important. Also, starting from about Mach 0.78 a diverging trend between FP and FPv predictions is found. At this point the predicted inviscid shock waves become too strong (now violating the FP assumptions) while viscous effects in the FPv formulation reduce their strengths (to keep having accurate steady state solutions) resulting in a correct prediction of the other side of the transonic dip with the sharp rise in the critical flutter speed index. In other words, viscous effects (included in the system Jacobian matrix) due to stronger shock/boundary layer interaction seem to become more significant than entropy and vorticity effects.

To support the observations, the inviscid/viscous coupling procedure in the FP formulation is exploited. Looking at the expression in Eq. (1), all matrix blocks (except A_{ss}) are split for the coupling to accommodate inviscid and viscous contributions in the fluid unknowns and their corresponding residuals, e.g. matrix block A_{ff} contains four subblocks. Then, individual subblocks are left out to estimate their importance for the stability analysis. In Fig. 7(b) three simulations using the FP baseline model are discussed with the first part of their labels indicating the steady state model and the second part indicating the contribution to the Jacobian matrix for the stability analysis. The simulation using an inviscid/viscous coupling for the

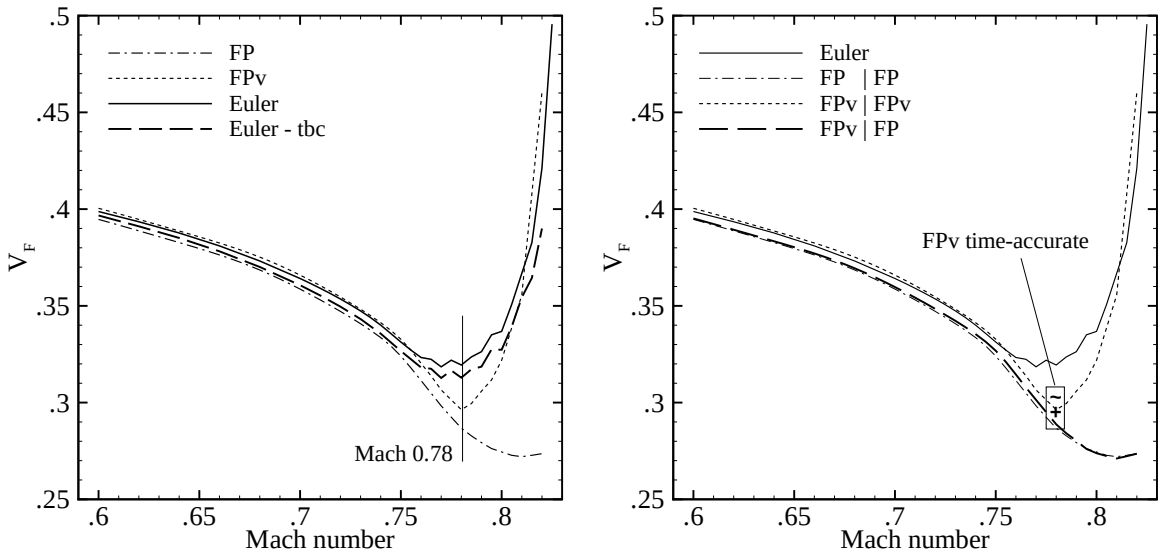

(a) Transpiration boundary condition (b) Jacobian blocks

Figure 7. Influences of both the transpiration boundary condition (tbc) and the Jacobian blocks for inviscid/viscous coupling on the predicted critical flutter speed index for NACA 0012 configuration.

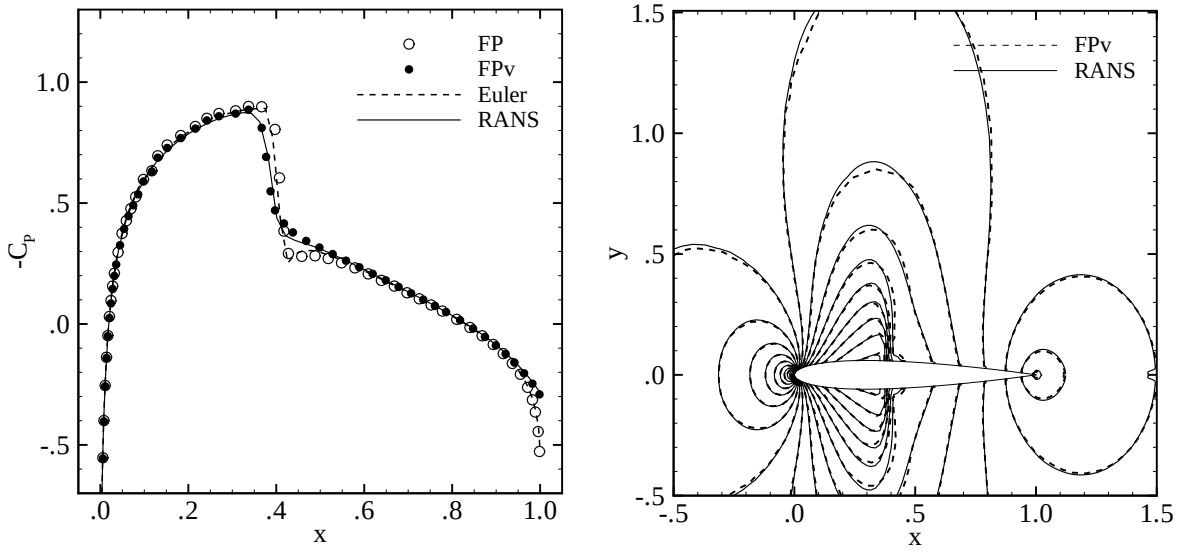

(a) Surface pressure distribution (b) Pressure field

Figure 8. Pressure distribution for NACA 0012 aerofoil and different flow models (M=0.78, α=0.0°, Re=5.0×10^6).

steady state but only the inviscid fluid subblock for the Schur complement matrix illustrates that, despite having the correct steady state, the inviscid instability boundary is predicted. Thus, the sensitivities of the important physics (in this case the viscous effects) need to be included in the matrix. Also, despite having the correct steady state compared to the Euler/RANS models, the sensitivity due to shock effects (entropy and vorticity production) is missing in the FP formulation and may cause the underprediction in the transonic dip minimum.

To summarize, having a correct steady state simulation does not immediately guarantee the correct prediction of the stability limit. More efforts will be needed for understanding to what extent either the missing physical content, such as shock effects, or the chosen discretisation of the flow models, such as the distinct upwind schemes, are the main factor in this discussion.

V. Coordinated Sampling

The cost to create the approximation model, i.e. the required number of samples to adequately represent the variation of the interaction matrix, is an important factor in the analysis especially for an expensive high fidelity flow model. The large number of samples as used, for instance, in Fig. 6 does not seem to be required to accurately predict the response surface near the instability. Sampling techniques can be exploited instead.[b] In Fig. 6, rectangular grid sampling has been applied. Latin hypercube (LH) sampling is considered as an improved version of random (Monte Carlo) sampling [48]. While random sampling creates parameter combinations independently (and possibly without providing additional information), LH sampling ensures that all parts of the parameter space are evenly represented. Therefore, each parameter dimension is divided into a specified number of non–overlapping bins of equal probability. One sample per dimension is randomly chosen from each bin and then randomly combined with the other parameter dimensions.

This approach, based on 8 and 32 samples, is presented in Fig. 9 for the FP flow model using the same NACA 0012 aerofoil configuration and a grid with 5k control volumes. Initially, four samples were placed at the corners of the parameter space in each case to avoid extrapolation while the remaining design points were generated (a priori) by LH sampling. The dimensions of the parameter space are defined to provide a good range for an initial blind search with the Mach number covering the region of interest (up to mild separation) and the frequency based on typical flutter frequencies (chosen from the normal mode frequencies). Looking at Fig. 9(a), even a few samples can approximate the target reasonably precisely. This observation is supported in Fig. 9(b) showing the critical flutter speed index as the true measure for the quality of the approximations while comparing to the full order reference solution. Using 8 samples a good starting point can be found to base a more detailed stability analysis on. Although one sample set gives results deviating considerably starting from about Mach 0.8, predictions based on 32 samples usually give better agreement.

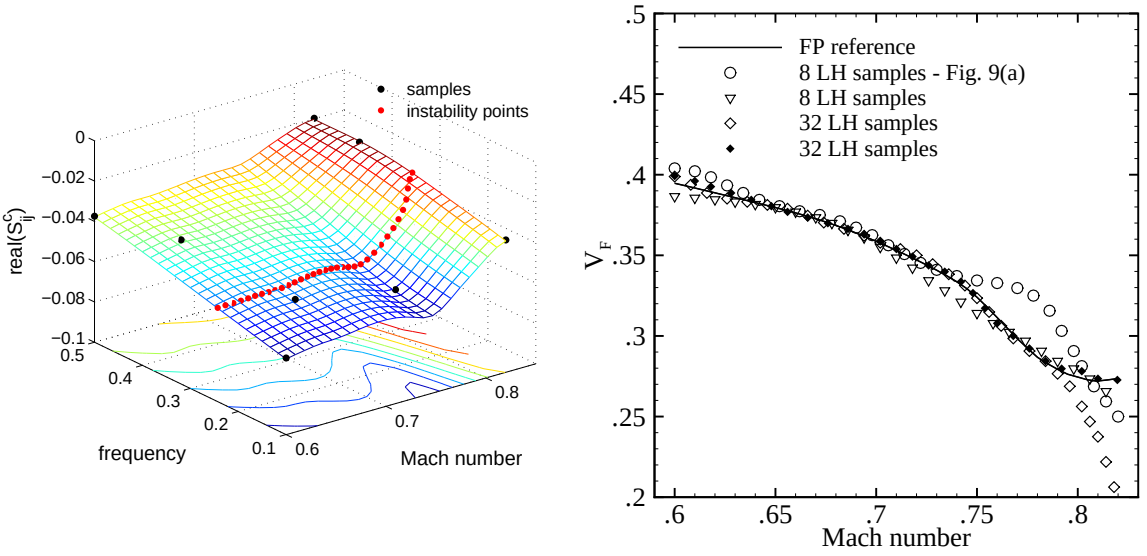

(a) Element real(S^c_{22}) for one set of 8 LH samples

(b) Critical flutter speed index

Figure 9. Latin hypercube (LH) sampling technique, using the FP flow model for NACA 0012 configuration, showing approximated element real(S^c_{22}) of Schur correction matrix including trace of instability and critical flutter speed index compared to a full order reference solution.

Instead of relying on these space–filling algorithms, information on the functional behaviour can be included to choose new sample locations a posteriori. The located maximum of the standard error for the current kriging prediction, readily available within the framework, defines a natural choice for a new sample. Iterating continues until a convergence criterion is satisfied. Results from this technique, referred to as mean squared error (MSE) sampling, are shown in Fig. 10. Initially, a number of LH samples is created to allow a first evaluation of the kriging model and to provide a somewhat filled parameter space. In the figure it is

[b]One sample here refers to the values of a complete interaction matrix at one combination of Mach number and frequency.

found that the response surface is well predicted with less irregularities compared to pure LH sampling with the same number of samples. It is remarked that MSE sampling is an improved (a posteriori) space–filling since the kriging error depends on the chosen correlation weighted by a function of the distance between samples. Thus, a new sample location is likely to be found near the point maximizing the distance to all surrounding samples while also adjusting to the level of correlation between the samples. The predicted critical flutter speed index, presented in Fig. 10(b), gives very good agreement to the reference solution.

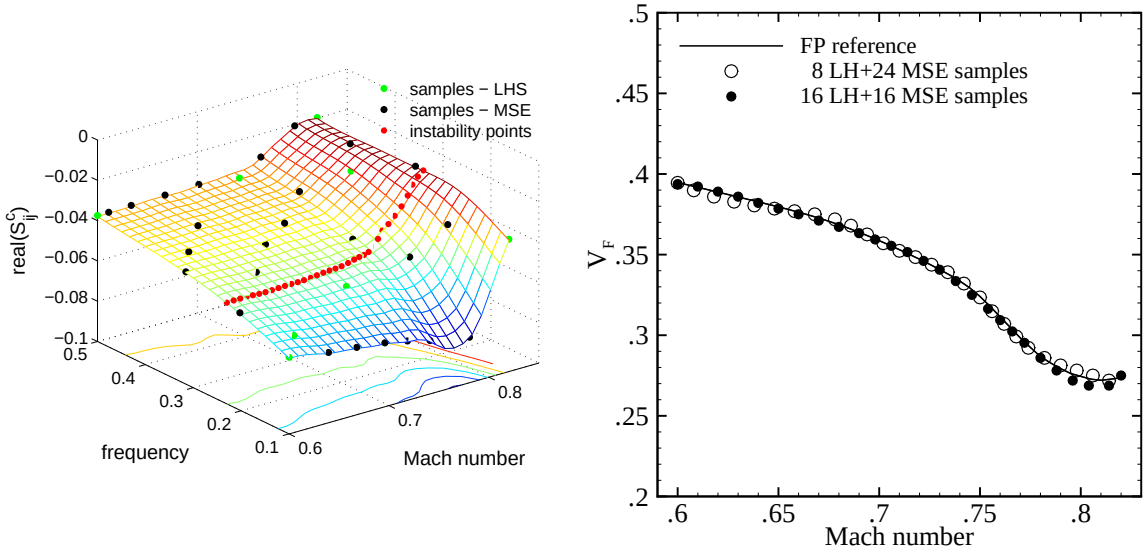

(a) Element real(S_{22}^c) for 8 LH plus 24 MSE samples

(b) Critical flutter speed index

Figure 10. Mean squared error (MSE) sampling technique, using the FP flow model for NACA 0012 configuration, showing approximated element real(S_{22}^c) of Schur correction matrix including trace of instability and critical flutter speed index compared to a full order reference solution.

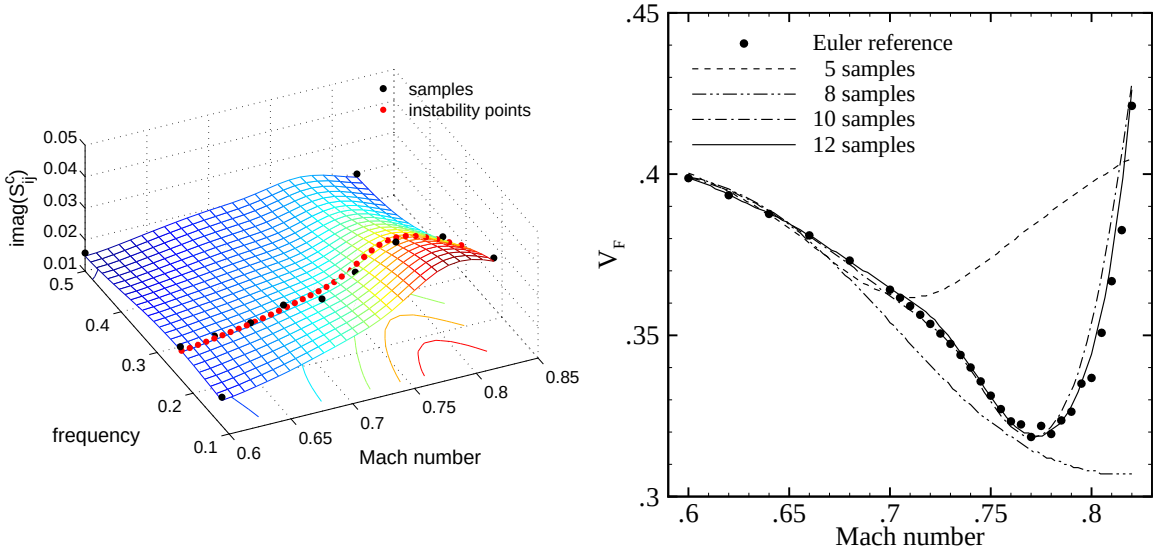

(a) Element imag(S_{22}^c) based on 12 samples

(b) Critical flutter speed index

Figure 11. Risk–based MSE sampling technique, using the Euler flow model for NACA 0012 configuration, showing approximated element imag(S_{22}^c) of Schur correction matrix including trace of instability and critical flutter speed index compared to a full order reference solution.

Latin hypercube sampling tries to fill the complete parameter space evenly, while with MSE sampling it is attempted to minimize the kriging error globally. Thus, looking at Figs. 9 and 10, it is found that many samples are redundant for the stability analysis. As the cost of running the Schur Newton solver using the approximation model is very low, it is useful to perform a complete stability analysis based on the current set of samples. Such a sampling approach proceeds by first defining the initial search space, in this example, with the four corner samples, and then evaluating the instability boundary. Locating the maximum of the kriging error along the current approximation to the instability boundary gives the new sample location. Iterating converges the solution to satisfy predefined stopping criteria, for instance, on the ℓ^2–norm of changes in successive flutter solutions and on the standard kriging error. This gives some measure of confidence in the prediction based on a distinct model in combination with the costs. The approach, referred to as risk–based MSE sampling, is illustrated in Fig. 11 for the Euler flow model using a grid with 15k control volumes for the NACA 0012 configuration. It can be seen that new samples are closely placed in the region where they strongly support the prediction. An accurate detection of the instability boundary is quickly obtained. The ten samples, being sufficient in this example to cover a complete sub- and transonic regime, correspond to the cost of about 20 steady state solves (including the simulation of steady flow fields) using the linear frequency domain approach for sample extraction. Here, evaluating the entire response surface within the initial search space is not attempted. As a consequence, mode tracking becomes inaccurate further away from the instability which, however, is a fair trade–off compared to the costs.

An alternative to the basic risk–based MSE sampling approach is shown in Fig. 12. The Isogai [49] benchmark case is known to exhibit multiple bifurcations for inviscid flow models in the deep transonic regime. Instead of using a bisection method on the reduced velocity $\bar{u}$ to locate the instability point, the roots of the Schur residual, obtained at low computational cost, are evaluated at all points on a mesh defined by Mach number and reduced velocity. Then, a threshold (sampling condition) is defined. In this study all mesh points at fixed Mach number having a change of sign in the eigenvalue's real part with varying reduced velocity are selected, thus, allowing multiple bifurcations. Alternative sampling conditions are possible. The selected location maximizing the kriging error gives a new parameter combination in Mach number and frequency as for the basic risk–based MSE sampling. In Fig. 12(b), showing the challenging instability boundary for the Isogai case, it is found that ten samples provide a good description of the (inviscid) transonic stability features, while more samples are required to predict the upper part (i.e. the second and third bifurcations) precisely. Some outliers in Fig. 12(a) are due to an intermediate approximation model not giving a converged solution at individual combinations of Mach number and flutter speed index placing the sample at the frequency search limit.

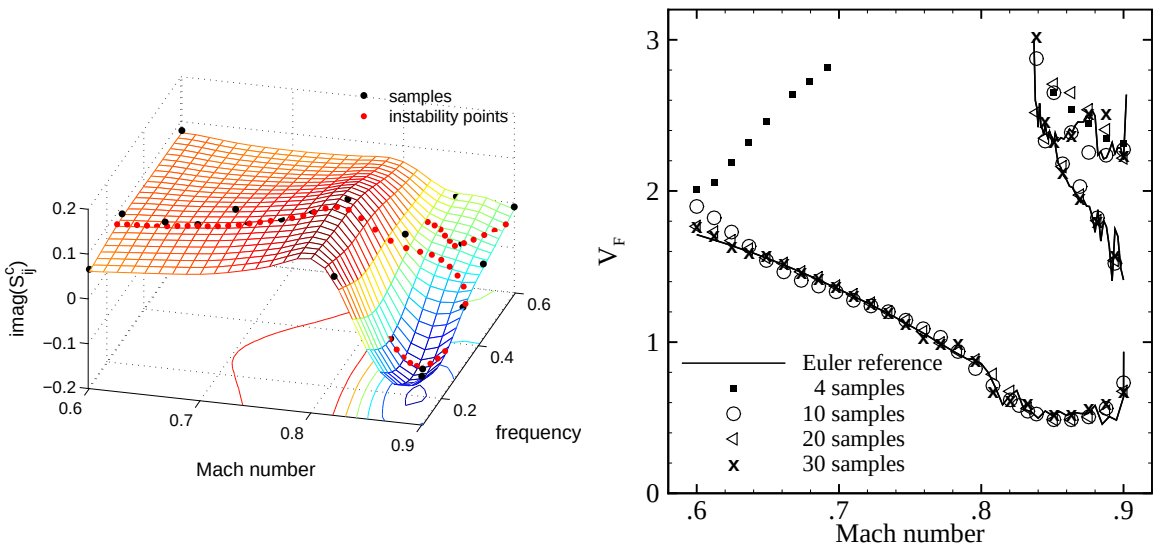

(a) Element imag(S^c_{22}) based on 20 samples

(b) Critical flutter speed index

Figure 12. Alternative risk–based MSE sampling technique, using the Euler flow model for Isogai [49] configuration, showing approximated element imag(S^c_{22}) of Schur correction matrix including trace of instability and critical flutter speed index compared to a full order reference solution.

There is another interesting aspect to the kriging formulation allowing the balance between local and global search for functional extrema [45]. The kriging model provides a mean (best) prediction of a response and a corresponding standard error. Then, a probability distribution can be given for the prediction. In Eq. (6) expand the interaction term in a first order Taylor series about the mean evaluation of the critical frequency ω_0 at fixed Mach number M,

$$S = S^s(\lambda, \bar{u}) + \check{S}^c(\omega_0) + \frac{\partial \hat{S}^c(\omega_0)}{\partial \omega_0}(\omega - \omega_0), \tag{7}$$

with the gradient of the mean prediction $\hat{S}^c(\omega_0)$ readily available from the kriging model. This is a good approximation looking at response variations in the frequency dimension. The value of ω_0 is found from a stability analysis based on mean values $\hat{S}^c$ of the kriging prediction for S^c. The elements of the matrix expression $\check{S}^c(\omega_0) = \mathcal{N}\big(\hat{S}^c(\omega_0), \varphi^2(\omega_0)\big)$ are assumed to be normally distributed with mean and variance given by their kriging approximation. Here, the matrix φ contains the standard error of the kriging prediction. Equation (7) models the uncertainty about the kriging approximated response $\hat{S}^c$ at an untried parameter combination (*not* the uncertainty due to physical effects). Then, a Monte Carlo simulation for random realisations of the term $\check{S}^c$ is done to propagate the uncertainty from the kriging model to the stability prediction. Also, an expected improvement function [45] is given for the evaluated critical flutter speed index, assumed to be normally distributed, to locate the minimum value (often corresponding to the transonic dip). This function takes the current best approximation of the extreme value and weights a possible improved minimum value by the corresponding probability density.

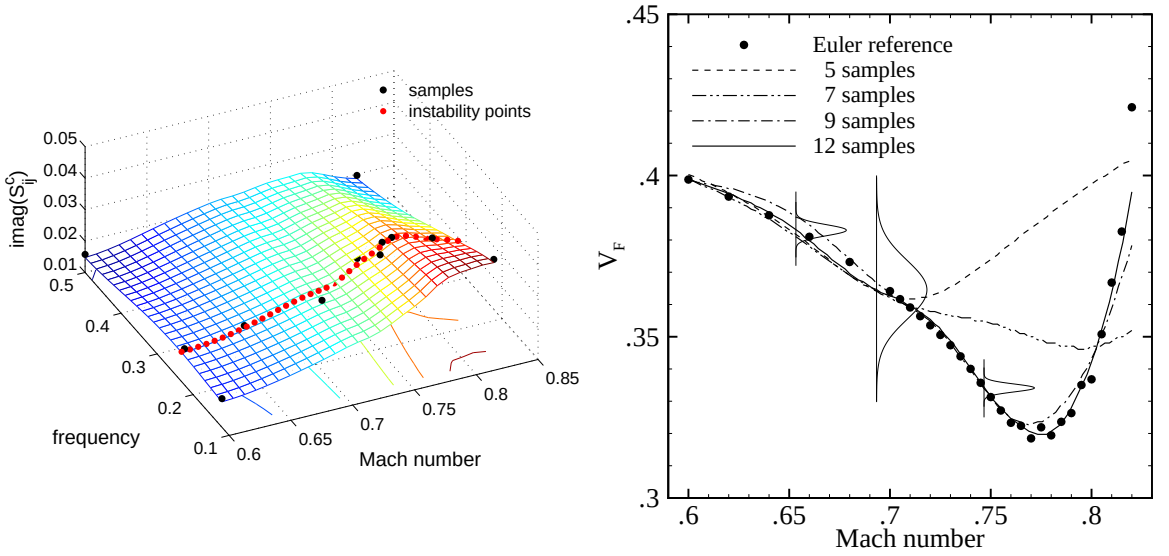

(a) Element imag(S^c_{22}) based on 12 samples

(b) Critical flutter speed index

Figure 13. Expected improvement (EI) sampling technique, using the Euler flow model for NACA 0012 configuration, showing approximated element imag(S^c_{22}) of Schur correction matrix including trace of instability and critical flutter speed index compared to a full order reference solution including response probability density functions.

The approach, referred to as expected improvement (EI) sampling, is illustrated in Fig. 13. Using intermediate stability results in finding new sample points (as done for risk–based MSE sampling), the samples gather around the converged flutter solution as seen in Fig. 13(a). However, it is obvious that more samples are placed in the region of the transonic dip since detecting the minimum in the critical flutter speed index is the objective of the applied EI sampling approach. This is desirable because more emphasis is consequently put on the nonlinear transonic regime rather than on the subsonic range. In Fig. 13(b) nine samples are sufficient to detect and predict the transonic dip accurately. The figure also includes (scaled) probability density functions for the critical flutter speed index at three Mach numbers for calculations based on 12 samples. Looking at the density function with the highest standard deviation, the idea of expected improvement is nicely described. Risk–based MSE sampling would place a new sample where the

standard deviation is highest (around Mach 0.7). Since the tail of the density function does not suggest an improvement in locating the minimum value of the critical flutter speed index (i.e. the probability to have a new minimum is very small), EI sampling ignores this location as a possible newly sampled point. Also, following engineering intuition, one would not expect the transonic dip at the lower Mach numbers. Expected improvement sampling is more expensive in finding a new sample location since a response distribution in the critical flutter speed index has to be evaluated for the range of Mach numbers. These costs remain constant though no matter how big the original problem becomes.

Summarizing, a blind search for aeroelastic instability starts with defining an initial search space in Mach number and frequency. Optionally, using LH sampling this space can then be filled evenly with more samples. To search for a complete range of the stability limit the risk–based MSE sampling approach is a convenient choice, whereas the EI sampling technique is preferred when the most critical region (i.e. the transonic dip) is the main concern. Having the steady state solutions, the cost for evaluating 12 samples, requiring $2n$ linear solves against the fluid system per sample using the linear frequency domain approach, for the approximation model to cover an entire Mach number range is equivalent to form the terms in the series expansion in Eq. (3) for the two normal modes of the aerofoil case at three individual Mach numbers, requiring $4n$ linear solves per mode and Mach number. This becomes more significant for cases with increasing number of considered normal modes. Also, the robustness issues of the *series method* for bigger frequency changes with varying independent parameter must be mentioned.

VI. Exploiting the Model Hierarchy

Following the preceding discussion, an appropriate sampling technique reduces the involved costs considerably in detecting the stability limit for an unknown configuration. The approach can be taken a step further. As mentioned before, the flow models of different fidelity, chosen in this study, usually predict similar features (as described by the Schur interaction term). In this sense, for instance, a response obtained by a FPv flow model is correlated with a RANS prediction as changes in a system parameter, such as Mach number, cause similar changes in the outcomes of the different flow models as illustrated in Fig. 6. Of course, the fundamental assumptions of both the FP formulation and the integral boundary layer formulation would hamper an accurate prediction compared to RANS. However, this predictive relationship can still be exploited.

To start with, a blind search using the expensive high fidelity model is avoided. The initial analysis using a cheaper model delimits the search space for aeroelastic instability and creates a general picture for a configuration. In addition, a relationship for the critical frequency of the form $\omega_F = \omega_F(M)$ can be given (for the analysis as described in this paper). This allows placing a few carefully selected high fidelity samples in presumed critical regions as predicted by the cheaper model. Figures 14 and 15 present an analysis exploiting the aerodynamic modelling hierarchy. The lower fidelity model is established by the FPv flow model whereas the RANS equations are used for the higher fidelity model. In Fig. 14 the instability boundary is shown as critical values of flutter speed index and frequency. Correspondingly in Fig. 15, one element of the interaction matrix is given for two different approaches to the kriging approximation based on an augmented set of samples details of which are discussed shortly. In addition, in Fig. 14 the predictions based on three different kriging approaches are included. A set of four RANS samples (i.e. four complete interaction matrices), selected according to the FPv prediction, is used with the sample distribution given in Figs. 14(b) and 15. Extracting all FPv samples in Fig. 6 using the linear frequency domain approach is less expensive than evaluating the few RANS samples using the nonlinear time domain approach. The FPv simulations were run on a grid with 5k control volumes, while the applied RANS grid has 20k volumes.

First, a kriging model based on these four samples was used and, as the results in Fig. 14 demonstrate, the small number of samples is inadequate for an accurate prediction. The distribution of samples in the $M-\omega$ parameter space along the instability boundary almost shows one–dimensional dependency on the Mach number with little change in the direction of frequency. This complicates significantly the creation of a kriging model with two input dimensions required for the stability analysis as discussed herein. Thus, it was found to be useful to augment the set of high fidelity samples by the lower fidelity corner points. This assumes that the initial search space is big enough to support the kriging model in the frequency dimension but not to adversely affect the approximation close to the instability. Then, a second kriging model, labelled "Kriging – aug.", based on the augmented data is formed. The resulting prediction shows a far better agreement compared to the reference solution based on the kriging model shown in Figs. 6(g) and 6(h).

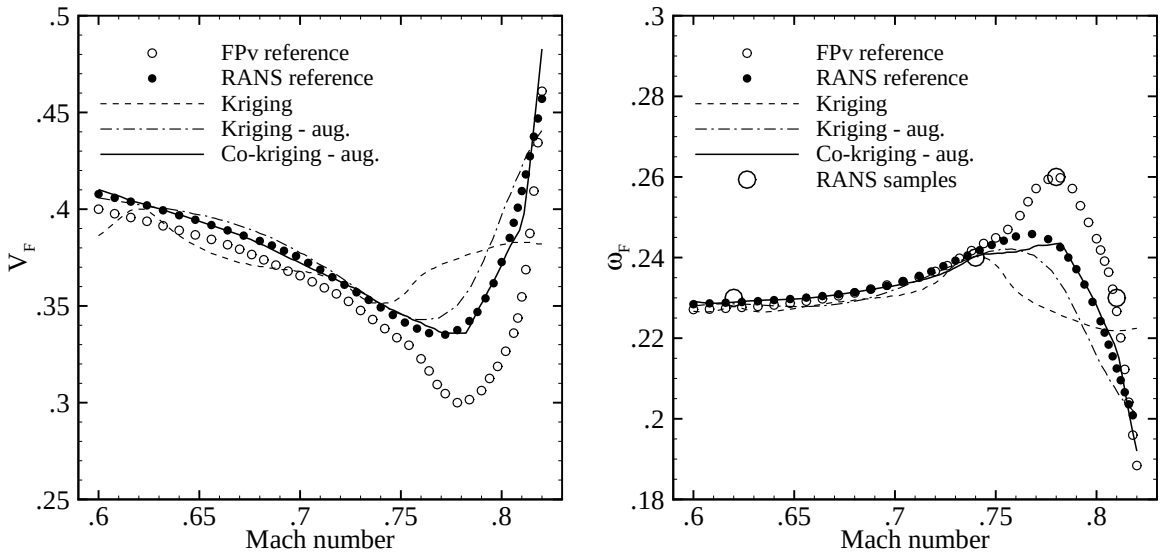

(a) Critical flutter speed index

(b) Critical frequency

Figure 14. Direct kriging and co–kriging techniques applied to aeroelastic stability analysis of NACA 0012 configuration showing critical values of flutter speed index and frequency.

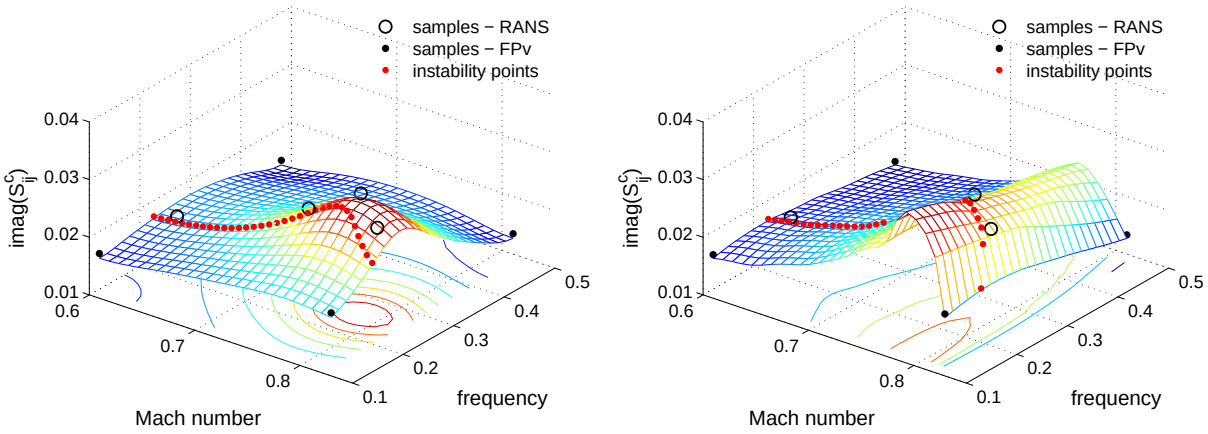

(a) Element imag(S^c_{22}) based on direct kriging

(b) Element imag(S^c_{22}) based on co–kriging

Figure 15. Direct kriging and co–kriging techniques applied to aeroelastic stability analysis of NACA 0012 configuration, using augmented sample set, showing approximated element imag(S^c_{22}) of Schur correction matrix.

Thirdly, the co–kriging approach to the approximation treats the lower fidelity response as a (correlated) co–variable to the higher fidelity prediction. Then, the input parameter space of the RANS samples (already augmented by the FPv corner samples) is extended by the FPv response given in Fig 6. This means, beside the dependence on Mach number and frequency, the approximation of the RANS–based response surface also depends on the FPv response which provides the trend information. Comparing Fig. 6(h) with Fig. 15(b) it is found that the response surface of the presented interaction element is reproduced well. Correspondingly, an accurate prediction of the instability boundary is found in Fig. 14. However, as seen in the previous paragraph, even a direct kriging model based on the augmented data set gives good results which corresponds to the earlier observation that the response surface close to the instability (as fairly given by the RANS samples) is essential for the stability prediction.

There is another interesting point which, however, is not presented in this paper. For systems with many relevant structural modes, the kriging approximation model of the cheaper flow representation can be exploited to perform a detailed sensitivity study of the configuration. This would provide information about both the dominant matrix elements and the dominant coupling mechanisms in the modes of the configuration. Consequently, high fidelity evaluations can be focused on these dominant interacting terms, i.e. elements of the Schur interaction matrix, rather than on the entire matrix.

Instead of estimating the stability limit over a range of Mach numbers, the most critical condition as found from a cheaper model can be chosen to place one expensive sample. In the vicinity of this critical location, the stability prediction continues as described using the kriging approximation based on a cheaper flow model, while the difference between the responses of higher and lower fidelity is used as constant shift added to the kriging predicted (lower fidelity) response of the interaction term.

VII. Conclusions and Outlook

The approach presented in this paper exploits the formulation of the Schur complement eigenvalue framework and builds an approximation model, using the kriging interpolation technique, for the interaction term of the Schur complement matrix based on samples of the full order model. A hierarchy of flow models is presented along with benchmark results. Ways to extract the samples are discussed and related issues such as shock–induced oscillations in the system response are considered. The approximation model applied to the structural model of a pitch and plunge aerofoil is analysed. Also, ideas to reduce the costs in constructing the approximation model are discussed. Here, a posteriori risk–based sampling approaches are tested, and the aerodynamic modelling hierarchy is exploited for model updating and data fusion.

While the basic Schur formulation, relying on steady flow simulations, is faster than common time–accurate approaches, the approximation model proves to be computationally more efficient than the basic formulation, despite the costs spent in the construction of the kriging model itself. Evaluating the Schur interaction matrix at discrete Mach numbers and frequencies is less expensive than directly using the full formulation since iterating on the full order system to converge the solution at a parameter combination is avoided, while iterating on the approximation model is very cheap. Also, competitive results are obtained with the model reduction. Another convenient aspect of the proposed method is the access to higher fidelity flow models in the aeroelastic stability analysis, such as Reynolds–averaged Navier–Stokes modelling, which has not been done before within the Schur framework. The method can be applied over a large range of Mach numbers avoiding pointwise time–accurate simulations to bracket the instability.

In future studies, the approach is being extended to accommodate more realistic three–dimensional cases. The dimension of the independent input variables in the kriging prediction can be increased to include different effects, such as aerostatic effects and possibly even structural parameters. Using the approach of artificial neural networks for the interpolation, instead of the kriging technique, to build the response surfaces of the interaction matrix is another interesting possibility.

Acknowledgments

This research has been supported by the European Union for the Marie Curie Centre of Excellence "ECERTA" under contract MEXT–CT–2006–042383.

References

[1] Friswell, M. I. and Mottershead, J. E., *Finite element model updating in structural dynamics*, Kluwer Academic Press, Dorndrecht, The Netherlands, 1995.

[2] Palacios, R., Climent, H., Karlsson, A., and Winzell, B., "Assessment of strategies for correcting linear unsteady aerodynamics using CFD or experimental results," *IFASD 2001–074*, 2001.

[3] Walters, R. W. and Huyse, L., "Uncertainty analysis for fluid mechanics with applications," Tech. Rep. NASA/CR–2002–211449, NASA Langley Research Center, Hampton, VA, 2002.

[4] Walters, R. W., "Towards stochastic fluid mechanics via polynomial chaos," *AIAA Paper 2003–0413*, 2003.

[5] Xiu, D. and Karniadakis, G. E., "Supersensitivity due to uncertain boundary conditions," *Int. J. Numer. Meth. Engng*, Vol. 61, 2004, pp. 2114–2138.

[6] Pettit, C. L., "Uncertainty quantification in aeroelasticity: recent results and research challenges," *Journal of Aircraft*, Vol. 41, No. 5, 2004, pp. 1217–1229.

[7] Beran, P. S., Khot, N. S., Eastep, F. E., Snyder, R. D., and Zweber, J. V., "Numerical analysis of store–induced limit–cycle oscillation," *Journal of Aircraft*, Vol. 41, No. 6, 2004, pp. 1315–1326.

[8] Schewe, G., Mai, H., and Dietz, G., "Nonlinear effects in transonic flutter with emphasis on manifestations of limit cycle oscillations," *Journal of Fluids and Structures*, Vol. 18, 2003, pp. 3–22.

[9] Dietz, G., Schewe, G., and Mai, H., "Experiments on heave/pitch limit–cycle oscillations of a supercritical airfoil close to the transonic dip," *Journal of Fluids and Structures*, Vol. 19, 2004, pp. 1–16.

[10] Dietz, G., Schewe, G., and Mai, H., "Amplification and amplitude limitations of heave/pitch limit–cycle oscillations close to the transonic dip," *Journal of Fluids and Structures*, Vol. 22, 2006, pp. 505–527.

[11] Dowell, E. H., Edwards, J. W., and Strganac, T. W., "Nonlinear aeroelasticity," *Journal of Aircraft*, Vol. 40, No. 5, 2003, pp. 857–874.

[12] Farhat, C., Geuzaine, P., and Brown, G., "Application of a three–field nonlinear fluid–structure formulation to the prediction of the aeroelastic parameters of an F–16 fighter," *Computers & Fluids*, Vol. 32, No. 1, 2003, pp. 3–29.

[13] Woodgate, M. A., Badcock, K. J., Rampurawala, A. M., Richards, B. R., Nardini, D., and deC Henshaw, M. J., "Aeroelastic calculations for the Hawk aircraft using the Euler equations," *AIAA Journal*, Vol. 42, No. 4, 2005, pp. 1005–1012.

[14] Lucia, D. J., Beran, P. S., and Silva, W. A., "Reduced–order modeling: new approaches for computational physics," *Progress in Aerospace Sciences*, Vol. 40, 2004, pp. 51–117.

[15] Amsallem, D. and Farhat, C., "Interpolation method for adapting reduced–order models and application to aeroelasticity," *AIAA Journal*, Vol. 46, No. 7, 2008, pp. 1803–1813.

[16] Bui–Thanh, T., Damodaran, M., and Willcox, K., "Proper orthogonal decomposition extensions for parametric applications in transonic aerodynamics," *AIAA Paper 2003–4213*, 2003.

[17] Morton, S. A. and Beran, P. S., "Hopf–bifurcation analysis of airfoil flutter at transonic speeds," *AIAA Paper 96–0060*, 1996.

[18] Morton, S. A. and Beran, P. S., "Hopf bifurcation analysis applied to deforming airfoils at transonic speeds," *AIAA Paper 97–1772*, 1997.

[19] Morton, S. A. and Beran, P. S., "Hopf–bifurcation analysis of airfoil flutter at transonic speeds," *Journal of Aircraft*, Vol. 36, No. 2, 1999, pp. 421–429.

[20] Badcock, K. J., Woodgate, M. A., and Richards, B. E., "Hopf bifurcation calculations for a symmetric airfoil in transonic flow," *AIAA Journal*, Vol. 42, No. 5, 2004, pp. 883–892.

[21] Badcock, K. J., Woodgate, M. A., and Richards, B. E., "Direct aeroelastic bifurcation analysis of a symmetric wing based on Euler equations," *Journal of Aircraft*, Vol. 42, No. 3, 2005, pp. 731–737.

[22] Woodgate, M. A. and Badcock, K. J., "Fast prediction of transonic aeroelastic stability and limit cycles," *AIAA Journal*, Vol. 45, No. 6, 2007, pp. 1370–1381.

[23] Badcock, K. J. and Woodgate, M. A., "Prediction of bifurcation onset of large order aeroelastic models," *AIAA Paper 2008–1820*, 2008.

[24] Marques, S., Badcock, K. J., Khodaparast, H. H., and Mottershead, J. E., "CFD based aeroelastic stability predictions under the influence of structural variability," *AIAA Paper 2009–2324*, 2009.

[25] Raj, P., "Computational uncertainty: Achilles' heel of simulation based aircraft design," AVT–147 Symposium on 'Computational Uncertainty in Military Vehicle Design', 2007.

[26] Badcock, K. J., Richards, B. E., and Woodgate, M. A., "Elements of computational fluid dynamics on block structured grids using implicit solvers," *Progress in Aerospace Sciences*, Vol. 36, 2000, pp. 351–392.

[27] Jameson, A., "Time dependent calculations using multigrid with applications to unsteady flows past airfoils and wings," *AIAA Paper 91–1596*, 1991.

[28] Osher, S. and Chakravarthy, S., "Upwind schemes and boundary conditions with applications to Euler equations in general geometries," *Journal of Computational Physics*, Vol. 50, 1983, pp. 447–481.

[29] van Leer, B., "Towards the ultimative conservative difference scheme. V. A second–order sequel to Godunov's method," *Journal of Computational Physics*, Vol. 32, 1979, pp. 101–136.

[30] Timme, S. and Badcock, K. J., "oFPfoil (v1.0) – User Guide," available online at http://cfd4aircraft.com/4downloads.php.

[31] Davis, T. A., "UMFPACK Version 5.4.0 user guide," Tech. Rep. TR–04–003 rev., Dept. of Computer and Information Science and Engineering, Univ. of Florida, Gainesville, FL, 2009, available at http://www.cise.ufl.edu/research/sparse/umfpack/.

[32] Holst, T. L., "Transonic flow computations using nonlinear potential methods," *Progress in Aerospace Sciences*, Vol. 36, 2000, pp. 1–61.

[33] Whitfield, D. L., "Analytical description of the complete turbulent boundary layer velocity profile," *AIAA Paper 78–1158*, 1978.

[34] Whitfield, D. L., Swafford, T. W., and Jacocks, J. L., "Calculation of turbulent boundary layers with separation and viscous–inviscid interaction," *AIAA Journal*, Vol. 19, No. 10, 1981.

[35] Swafford, T. W., "Analytical approximation of two–dimensional separated turbulent boundary layers," *AIAA Journal*, Vol. 21, No. 6, 1983, pp. 923–926.

[36] Drela, M. and Giles, M. B., "Viscous–inviscid analysis of transonic and low Reynolds number airfoils," *AIAA Journal*, Vol. 25, No. 10, 1987, pp. 1347–1355.

[37] Schlichting, H. and Gersten, K., *Boundary–layer theory*, Springer–Verlag, Inc., Berlin, Germany, 8th rev. and enl. ed., 2000.

[38] Lighthill, M. J., "On displacement thickness," *Journal of Fluid Mechanics*, Vol. 4, 1958, pp. 383–392.

[39] Cook, P. H., McDonald, M. A., and Firmin, M. C. P., "Aerofoil RAE 2822 – Pressure distributions, and boundary layer and wake measurements," Tech. Rep. AGARD AR 138, 1979.

[40] Fung, Y. C., *An introduction to the theory of aeroelasticity*, John Wiley & Sons, Inc., New York, NY, 1955.

[41] Bekas, C. and Saad, Y., "Computation of smallest eigenvalues using spectral Schur complements," *SIAM J. Sci. Comput.*, Vol. 27, No. 2, 2005, pp. 458–481.

[42] Oran Brigham, E., *The fast Fourier transform and its applications*, Prentice–Hall, Englewood Cliffs, NJ, 1988.

[43] Timme, S. and Badcock, K. J., "Oscillatory behavior of transonic aeroelastic instability boundaries," *AIAA Journal*, Vol. 47, No. 6, 2009, pp. 1590–1592.

[44] Sacks, J., Welch, W. J., Mitchell, T. J., and Wynn, H. P., "Design and analysis of computer experiments," *Statistical Science*, Vol. 4, No. 4, 1989, pp. 409–435.

[45] Jones, D. R., Schonlau, M., and Welch, W. J., "Efficient global optimization of expensive black–box functions," *Journal of Global Optimization*, Vol. 13, No. 4, 1998, pp. 455–492.

[46] Ghoreyshi, M. and Badcock, K. J., "Accelerating the numerical generation of aerodynamic models for flight simulation," *AIAA Journal*, Vol. 46, No. 3, 2009, pp. 972–980.

[47] Hassig, H. J., "An approximate true damping solution of the flutter equation by determinant iteration," *Journal of Aircraft*, Vol. 8, No. 11, 1971, pp. 885–889.

[48] McKay, M. D., Conover, W. J., and Beckman, R., "A comparison of three methods for selecting values of input variables in the analysis of output from a computer code," *Technometrics*, Vol. 21, No. 2, 1979, pp. 239–245.

[49] Isogai, K., "Transonic–dip mechanism of flutter of a sweptback wing: part II," *AIAA Journal*, Vol. 19, No. 9, 1981, pp. 1240–1242.